When anatase nanoparticles become bulk-like: Properties of realistic TiO_2 nanoparticles in the 1 – 6 nm size range from all electron relativistic density functional theory based calculations

Oriol Lamiel-Garcia,[a] Kyoung Chul Ko,[ab] Jin Yong Lee,[b]
Stefan T. Bromley,[ac] Francesc Illas[a*]

[a)]*Departament de Ciència de Materials i Química Física & Institut de Química Teòrica i Computacional (IQTCUB), Universitat de Barcelona, C/ Martí i Franquès 1, 08028 Barcelona, Spain.*

[b)] *Department of Chemistry, Sungkyunkwan University, Suwon 16419, Korea.*

[c)] *Institució Catalana de Recerca i Estudis Avançats (ICREA), 08010 Barcelona, Spain.*

Abstract

All electron relativistic density functional theory (DFT) based calculations using numerical atom-centered orbitals have been carried out to explore the relative stability, atomic and electronic structure of a series of stoichiometric TiO_2 anatase nanoparticles explicitly containing up to 1365 atoms as a function of size and morphology. The nanoparticles under scrutiny exhibit octahedral or truncated octahedral structures and span the 1- 6 nm size range. Initial structures were obtained from a Wulff construction, thus exhibiting the most stable (101) and (001) anatase surfaces. Final structures were obtained from geometry optimization with full relaxation of all structural parameters using both generalized gradient approximation (GGA) and hybrid density functionals. Results show that, for nanoparticles of a similar size, octahedral and truncated octahedral morphologies have comparable energetic stabilities. The electronic structure properties exhibit a clear trend converging to the bulk values as the size of the nanoparticles increase but with a marked influence of the density functional employed. Our results suggest that electronic structure properties, and hence reactivity, for the largest anatase nanoparticles considered in this study will be similar to those exhibited by even larger mesoscale particles or by bulk systems. Finally, we present compelling evidence that anatase nanoparticles become effectively bulk-like when reaching a size of ~20 nm diameter.

1. Introduction

Titanium dioxide (TiO_2) nanoparticles are at the heart of large number of technological applications,[1] including solar cells[2,3], environmental clean-up,[4,5] self cleaning surfaces[6] and photocatalysis.[7-10] In particular, H_2 production from photocatalytic water splitting using TiO_2 nanoparticles[11,12] constitutes a promising clean and sustainable alternative to fossil fuels. Unfortunately, the rather large band gap (> 3.0 eV)[13] of the most common polymorphs of titanium dioxide (anatase, rutile and brookite) means that ultraviolet (UV) radiation is required for electronic excitation. This hinders general use as only ~10% of the incoming photons from sunlight have enough energy to be absorbed, and hence to participate in the photocatalytic process. Suitable modifications of titanium dioxide are thus actively being sought to overcome this constraint.

Several strategies, from nanostructuring1,[14] to doping with different types of elements,[15-17] have been proposed to reduce the band gap of TiO_2 so as to render the materials photocatalytic active under sunlight. The metastable anatase phase has been found to be stable in the form of nanoparticles. In turn these nanoparticles exhibit the highest photocatalytic activity, including water splitting reaction under certain conditions,[2,11,12,18-22] yet with too low activity under sunlight. The origin of the higher photocatalytic activity of anatase nanoparticles is largely unknown and likely to be the result of many factors including morphology, size and possibly the presence of point defects and/or adsorbates. Thus, new techniques have been developed aimed at controlling the shape and size of anatase nanoparticles with the goal of optimizing their photocatalytic activity.[23] Nevertheless, experimental conditions make it difficult to discern between the different effects of size and shape and those introduced by the synthesis conditions.

To complement experiments, theoretical models can be used to investigate the effect of different morphologies for a given composition, or vary the composition for a given morphology. A large amount of useful information has been gathered from electronic structure calculations of extended models of TiO_2 bulk polymorphs, including defects and/or dopants,[24-33] and of several well-defined surfaces.[34-36] However, these models lack effects arising from the finite size and shape of the TiO_2 nanoparticles. To take these effects into account requires explicitly modeling $(TiO_2)_n$ nanoparticles which is computationally expensive and so far largely limited to the electronic ground state

and small clusters with *n* in the 8-38 range.[37-45] The study of these species results in useful information although one must realize that rather small to moderately large $(TiO_2)_n$ nanoclusters typically exhibit a significant number of non-bulk-like energetically low lying isomers. Since this implies that experimental measurements may provide information over an ensemble of particles rather than on the most stable structural ground state, it is necessary to investigate the properties of different isomers of TiO_2 nanoparticles. This is analogous to the bulk case of TiO_2 polymorph engineering, where similarly energetically stable yet distinct crystal structures lead to different modifications of band edges and hence band gaps due to varying local coordination.[46]

The ground state and excited electronic structure of specific low energy $(TiO_2)_n$ non-bulk-like clusters in the size range n =1-15 have been studied in detail,[38,44] but information regarding larger particles is almost inexistent with the exception of a recent study by some of us dealing with ground and excited states of small TiO_2 clusters including the most stable isomers and the low lying ones and also considering larger anatase bulk-cut $(TiO_2)_n$ particles with n up to 84.[47] The transition from nanoclusters, without a regular atomic structure, to nanocrystals exhibiting the crystal structure of the known polymorphs has also been theoretically estimated recently and results indicate that anatase-like crystallinity emerges in titania nanoparticles of approximately 2–3 nm diameter.[48]

To help close the gap between nanoclusters and periodic models, Barnard et al.[49] developed a self-consistent tight-binding (SCTB) model that was found to be able to mimic the results obtained from density functional theory (DFT) based calculations of a moderately sized $(TiO_2)_{35}$ nanoparticle. These authors subsequently employed this SCTB approach to investigate the relative stability and atomic structure of $(TiO_2)_n$ anatase-like particles having different realistic bulk-cut morphologies exhibiting the lowest energy surfaces with n up to 455 (i.e. 1365 atoms). Unfortunately, the computational burden required to carry out explicit density functional theory based calculations for such large systems prevented reaching a more accurate description and the details of the electronic structure based properties of these large nanoparticles remain unknown. Nevertheless, the advent of new powerful supercomputers containing thousands of cores together to the existence of newly developed computational codes which are able to fully exploit this architecture should provide the appropriate framework to undertake this challenge. The aim of the present work is precisely to

provide a detailed study of the atomic and electronic structure of realistic $(TiO_2)_n$ nanoparticles, encompassing the models used by Barnard et al.[49] among others, and hence explore the convergence of stability and electronic structure related properties as a function of size and shape using a unified, consistent, and numerically accurate theoretical approach.

2. Computational details

The DFT based calculations for the TiO_2 nanoparticles described in this study were carried out using the highly parallel FHI-AIMS code which is able to handle thousands of atoms with O(N) scaling.[50,51,52] The calculations explicitly include all electrons and relativistic effects are accounted for at the zeroth order regular approximation (ZORA)[53,54]. The atomic structure of the different nanoparticles considered in the present work were optimized at the DFT level using the Perdew-Bruke-Ernzerhof[55] (PBE) implementation of the Generalized Gradient Approximation (GGA) using a light-tier-1 numerical atom-centered orbitals (NAO) basis with quality similar to that obtained with valence triple-ζ plus polarization Gaussian Type Orbitals (GTO) as illustrated in the next section. In most cases, tight-binding optimized structures[49,56] were used as starting points which facilitates the convergence of the geometry optimization. The energy threshold for self consistency was chosen as 10^{-5} eV. In the geometry optimization, all atoms were allowed to relax until the atomic forces were smaller than 0.001 eV/Å.

To improve the description of the electronic structure of these systems and to overcome the well known underestimation of the band gap associated with calculations using GGA functionals,[25,57] we performed single point calculations using the optimized PBE structures with the PBE0 and PBEx hybrid functionals. The latter includes an empirically chosen 12.5% of Hartree Fock exchange (instead of the 25% of the PBE0) so as to properly describe the electronic structure of stoichiometric and reduced rutile and anatase polymorphs/nanoparticles of TiO_2.[58,59] The single point calculations with the hybrid functionals were carried out using the same light-tier1 basis set and the same electronic convergence criteria of 10^{-5} eV for the total energy.

All calculations presented in this work were carried out the Marenostrum supercomputer of the Barcelona Super Supercomputer Center (BSC) using 1024 cores with a time limitation of 72 hours per run. Within this constraint the hybrid (PBEx and

PBE0) DFT based calculations for the ground state of the largest nanoparticle and the PBE open shell spin polarized calculations for the cation and anion were unfeasible. Yet, the trends from the series of calculations lead to meaningful and sound conclusions as described in detail in the forthcoming sections.

3. Defining the TiO_2 anatase nanoparticles

Ten different stoichiometric $(TiO_2)_n$ nanoparticles have been modeled with *n* ranging from 10 to 455 TiO_2 units hence containing up to 1365 atoms. The initial structure of these nanoparticles was obtained via Wulff constructions.[60,61] This approach relates the shape of the nanoparticle to the area of the surfaces exposed and of their relative stability. For the anatase phase of titania, the two most stable surfaces are the (101) and (001) respectively.[62] Restricting the morphology of the three-dimensional nanoparticles to those exhibiting these two surfaces leads to two kind of structures, a first set exhibiting only the (101) surface and displaying octahedral (O_h) symmetry and a second set simultaneously exhibiting (101) and (001) surface displaying a truncated octahedral (TO_h) shape. In the following we will refer to both sets of nanoparticles as O_h and TO_h and are schematically shown in Figure 1.

Lu *et al.*[63] have been able to stabilize anatase nanoparticles exhibiting a large amount of the less stable (001) surface using fluorine. This finding has been later rationalized from DFT calculations and *ab initio* thermodynamics showing that F stabilizes the (001) surface and destabilizes the (101) ones.[64] Lu *et al*. also found that particles exhibiting the (001) facets present a higher photocatalytic activity than the nanoparticles presenting (101) surfaces only. This justifies the choice of nanoparticles studied which are displayed in Figure 2. The dimensions of these nanoparticles are between 1.3-6.1 nm high and 0.5-3 nm wide as measured from nucleus to nucleus or 1.6-6.4 nm high and 0.8-3.3 nm wide considering twice the O (1.52 Å) van der Waals radii,[65] as suggested by other authors.[66] Clearly, the size and shape of the nanoparticles studied in this work approach the size of experimentally synthesized nanoparticles used to probe photocatalytic water splitting.[23]

4. Results and discussion

Assessing the quality of the NAO basis set used

To assess the quality of the light-tier1 NAO basis set we compare the PBE total energy of the Ti atom and of the O_2 and TiO_2 molecules with those obtained using the widely used standard 6-311G** and TZVP basis sets. Table 1 reports the calculated energies corresponding to the formation of the TiO_2 molecule from Ti and O_2. For a proper comparison, the NAO results in Table 1 have been calculated without taking the relativistic effects into account. The calculations for the two molecules were carried out at the experimental geometry.

Results in Table 1 show that the energies obtained with the NAO light-tier1 basis set are always lower than those obtained with the 6-311G** GTO basis set by at least by 0.004 Hartrees and slightly higher than those obtained with the TZVP GTO basis set. Consequently, one can safely conclude that this NAO basis set is of triple-z plus polarization quality which provides a good compromise between accuracy and computational cost, especially given the large size of the systems treated in the present work and the high computational cost of calculations with hybrid density functionals.

Stability and atomic structure as a function of size, shape and functional.

In this section we analyze the convergence of relative stability and structure of the modeled nanoparticles, as function of size, shape taking also into account the effect of the DFT method used. First, we note that the optimization of the bulk cuts nanoparticles preserves the initial shape with well defined surfaces except in the smallest particles. In the case of the O_h particles, two different types of nearly degenerate local minima are found differing essentially in the position of the two apical oxygen atoms. In one type, the apical Ti-O bond preserves its direction as in the bulk structure, whereas in the other the Ti-O apical bond is tilted relative the long axis of the nanoparticle (see Figure 3). Nevertheless, for each of the O_h nanoparticles, the difference of energy per TiO_2 unit relative to anatase bulk ($\Delta E/n$) between these two stable geometries is minor (~0.009 eV/unit) except for the case of the smallest $(TiO_2)_{10}$ nanoparticle where, as expected, the small size implies large surface reconstruction/distortion effects leading to a larger energy/unit difference (0.12 eV/unit). Because of the small difference in the energy/unit of these two types of isomers (see Figure S1 in the supporting information), further analysis of the stability respect to the

size and the functional used will focus on the structures with the tilted apical Ti-O bonds. Results regarding the more symmetric local minima are provided in the Supporting Information.

Figure 4 plots the ΔE/n values for the optimized $(TiO)_n$ structures of the O_h and O_hT nanoparticles as obtained from calculations using the PBE functional. For comparison Figure 4 also reports the corresponding ΔE/n values for the unrelaxed bulk cut structures as well as for the some of the structures as relaxed from the tight-binding method of Barnard et al.[49] which were made available by these authors. Figure 4 shows that, in all cases, ΔE/n drops rapidly with size especially in the range of the smaller nanoparticles; the largest energy decrease of 0.47 eV/unit corresponding to the increase in nanoparticle size from $(TiO_2)_{10}$ to $(TiO_2)_{35}$. With further increases nanoparticle size, ΔE/n continues to decrease asymptotically with the decrease in ΔE/n being only 0.06 eV/unit when going from $(TiO_2)_{286}$ to $(TiO_2)_{455}$. Within the nanoparticle size range we consider ΔE/n is still significant due to the presence of terminating surfaces which necessarily introduce an energy cost relative to the infinite bulk. The ΔE/n values by PBE for fully relaxed O_h and TO_h particles approximately follow the same curve in spite of the fact that the former contains (101) facets only and the latter includes also two less stable (001) facets. This is also clear from the formation energy plots in Figure S2 calculated with respect to Ti(s) and O_2(g) where values for O_h and TO_h particles follow the same trend.

From Figure 4 the variation in ΔE/n produced by relaxation of the atomic structure from the bulk cut to the PBE optimized structure can also be observed. This relaxation energy is very large for the smaller particles and asymptotically decreases for the larger ones as their internal structure converges to that of the bulk. Figure 4 also shows that the relaxation is much smaller when the initial structure has been previously optimized using the tight binding method of Barnard et al.[49] although further relaxation is still required to obtain the PBE minimum energy structure. In this sense, the tight binding method can be regarded as an efficient and economic way to provide suitable starting structures for subsequent more accurate calculations.

In order to assess the influence of the density functional on the relative stability of the nanoparticles modeled, we have calculated the energies of the nanoparticles using the PBEx and PBE0 functionals using fixed geometries obtained from optimizations at

the PBE level. For the relatively large nanoparticles considered in the present work, geometry optimization with the hybrid functionals is excessively demanding. Calculations with the hybrid functionals were excessively demanding for the $(TiO_2)_{455}$ particle and some PBEx and PBE0 results for this particle have been extrapolated from corresponding data calculated for the $(TiO_2)_{286}$ nanoparticle. An indication of the influence of the functional is provided by comparing the change in ΔE/n when going from the original bulk cut to the PBE-optimised structure for each functional. For PBE, this change in ΔE/n for $(TiO_2)_{10}$ is 1.26 eV/unit whereas for $(TiO_2)_{455}$ the corresponding ΔE/n decrease is about 0.28 eV/unit. The corresponding values for the PBEx hybrid functional are 1.39 eV/unit and 0.32 eV/unit and for the PBE0 functional 1.54 eV/unit and 0.39 eV/unit, respectively. The discussion so far relied on the structures optimized with the PBE functional. In absence of polarons,[67] as is the case here, PBE and PBEx lead to the same optimized structure as proven for both stoichiometric anatase and rutile.[58] Hence we can safely assume that for the stoichiometric particles under scrutiny the PBEx and PBE0 functionals will also lead to almost equivalent optimized structures. Consequently, it is acceptable to claim that trends in ΔE/n are rather independent of the density functional method used. Nevertheless, for a given particle, ΔE/n values decrease from PBE to PBEx and followed by the PBEx and PBE0 subsequently. The effect of the functional is a consequence of the higher localization of the molecular orbitals with increasing the amount of non-local Fock exchange in the functional.

To assess the convergence of structure with respect to the size of the nanoparticles we focus now on two structural parameters: (i) the average Ti-O distance and (ii) the average coordination of the Ti and O atoms. In both cases we take the values of bulk anatase as the converged limit for large nanoparticles. The smallest $(TiO_2)_n$ nanoparticles with $n < 35$ have an average Ti-O distance significantly below the bulk value but which rapidly converges to the bulk value as the size of the nanoparticles increases (Figure 5, top panel). A similar trend is found for the coordination of the Ti and O atoms but in this case the average coordination for Ti (Figure 5, middle panel) and O (Figure 5, bottom panel), converges to the bulk value more slowly. This is a result of the presence of a significant proportion of surface atoms always exhibiting lower coordination than those in the bulk.

Electronic structure related properties as a function of size, shape and functional.

One of the main features of TiO_2 is its photocatalytic activity, which is necessarily directly related to the electronic structure of the material in its different forms. Here, we discuss the electronic structure of the nanoparticles again focusing on the influence of size and shape and taking into account the effect of the choice of density functional. In particular we investigate the band gap of these materials and consider both the optical and electronic gap of the different $(TiO_2)_n$ nanoparticles following the strategy employed recently by Cho *et al.*[47] In all cases we use the anatase bulk values for the band gap as reference. This is justified since surface effects on the band gap of anatase have been reported to be very small. For instance, for TiO_2 nanoparticles with a diameter of 7.6 to 24 nm, the band bending from the center to the surface is only 0.004 eV only.[68]

The optical gap (O_{gap}) corresponds to the energy needed to excite an electron from the highest occupied molecular orbital (HOMO) energy level to the lowest unoccupied molecular orbital (LUMO) and is experimentally measurable from optical spectroscopy. On the other hand, the electronic gap (E_{gap}) is defined as the energy difference between the vertical ionization potential (VIP) and the vertical electron affinity (VEA) and is measured with the help of photoemission and inverse photoemission experiments. For an ideal infinite system with well delocalized valence and conduction bands both values coincide (i.e. in the absence of excitons). In fact, small exciton-like excitations have been found in rutile and anatase but the corresponding excitation energies are of the order of a few meV only. [69-71] In the case of relatively small finite systems O_{gap} is lower than E_{gap} because of the electrostatic stabilization of the electron-hole pair interaction in the exciton state. The difference between these two energy gaps is commonly defined as the exciton binding energy and provides a measure of how bulk-like a given nanoparticle of a certain size is with respect to its electronic structure.[47]

Let us start with the trends exhibited by O_{gap} which has been calculated simply as the energy difference of the corresponding Kohn-Sham energies. This is of course an approximation since an accurate treatment of the HOMO-LUMO excitation would require configuration interaction, time dependent DFT (TD-DFT), or GW many body quasi particle calculations. These levels of calculation are unfeasible for systems of the size considered in the present work. As such, the usual approach to estimating the band

gap of bulk solids involves using the Kohn-Sham energy eigenvalues from band structure calculations. Since the main purpose of the present work is to explore to convergence of O_{gap} towards the bulk it is reasonable to compare O_{gap} values for the nanoparticles and for the bulk using this widely used approach. This methodological choice is also justified from explicit TD-DFT calculations of the lowest singlet to singlet transition on $(TiO_2)_{35}$ and $(TiO_2)_{84}$ particles showing that, for a given functional, the HOMO-LUMO gap follow the same trends as those gaps obtained from TD-DFT.[47] However, because of the well known effect of the density functional on the position of the Kohn-Sham energy levels, also evidenced in recent work,[58] O_{gap} values have been obtained using the PBE, PBEx and PBE0 functionals and results for the O_h set of particles are summarized in Figure 6. Here, we recall that PBE severely underestimates the anatase experimental band gap of 3.2 eV, PBE0 overestimates it, and PBEx has been empirically adjusted to reproduce the experimental value for bulk TiO_2.[58] We note that the PBEx calculated O_{gap} of $(TiO_2)_{84}$ and $(TiO_2)_{455}$ particles with O_h morphology, corresponding to nanoparticles with 3nm and 6 nm apical diameters, are consistent with the experimentally estimated O_{gaps} of anatase nanoparticles with 3nm and 6 nm sizes assumed to have a spherical shape.[72] The calculated and experimental O_{gap} values are 3.61 eV and 3.50 eV for the 3nm nanoparticle and 3.34 eV and 3.34 eV for the 6nm one respectively. Hence, it appears that the PBEx functional also predicts reasonable O_{gap} values for TiO_2 nanoparticles. The same trend between functionals is observed for the O_{gap} values in Figure 6 where the most salient feature is perhaps the weak dependence of this quantity with respect to nanoparticle size This confirms that the electronic structure converges faster than the energy ($\Delta E/n$) related properties.

Figure 6 also reports the E_{gap} values for the O_h set of particles as obtained with the three different considered functionals. The results in Figure 6 show that E_{gap} values are also strongly dependent on the functional used, but also that they are markedly dependent on the particles size. As found for O_{gap}, lower values are obtained when using the PBE functional, higher energies for PBE0, with those corresponding to the PBEx functional in between. With respect to O_{gap}, the E_{gap} values rapidly decreases and asymptotically converge to the values of the anatase bulk band gap. For comparison and to assess the influence of the shape of the nanoparticle in this important property, Figure 7 collects the O_{gap} and E_{gap} values for the complete set of particles studied as predicted from the calculations using the PBEx hybrid functional[58] (the results for the largest particle are extrapolated as indicated above). Analysis of Figure 7 shows that, as far as

electronic structure is concerned, size dominates over shape. However, for a given size O_{gap} and E_{gap} noticeably vary with shape suggesting that it may be able to tune the electronic properties by modifying the nanoparticle morphology.

Finally, we focus on the exciton binding energy (ΔE_{ex}) defined as E_{gap}-O_{gap}. The magnitude of ΔE_{ex} provides a direct measure of convergence of electronic properties towards the bulk since, in absence of excitons as is the case in TiO_2,[69-71] the magnitude of ΔE_{ex} must tend to zero. Figure 8 plots ΔE_{ex} as a function of the number of TiO_2 units in the nanoparticles. Since E_{gap} decreases sharply with size and O_{gap} decreases more gradually, ΔE_{ex} exhibits a decreasing trend with size moving from energy values of about 3 eV at the PBEx level to less than 1 eV for the largest ones. This latter value fits well with predictions based on extrapolating results from smaller particles.[47] In addition, the present results allow one to define the size at which the TiO_2 nanoparticles will exhibit a bulk electronic structure. To this end, and following the strategy used in our previous work,[47] Figure 9 plots ΔE_{ex} for the $(TiO_2)_n$ particles with O_h morphology as a function of $n^{-1/3}$. Consistent with results of previous work,[47] the data in Figure 9 follow linear trends. The present PBE0 and PBEx fit lines lying in between those for smaller particles predicted by non relativistic B3LYP calculations within a standard GTO basis set of 6-31G(d) quality, and the same B3LYP results scaled down by 20% to empirically correct for the B3LYP overestimate of band gap of anatase. The linear plots in Figure 9 allows one to make a prediction of the number of TiO_2 units a particle should have to have an exciton shift within the limits of accuracy of experiment (taken to be approximately ±0.1 eV). Thus, assuming that an exciton shift of or smaller than 0.2 eV is indicative of bulk behavior, the trends in Figure 9 indicate that this limit is reached by O_h particles of 22810, 15000 and 10218 TiO_2 units for the PBE0, B3LYP and PBEx hybrid functionals, with a clear trend following the amount of Fock exchange (25, 20 and 12.5%) included in the functionals. In terms of TiO_2 units this may appear as a rather broad range but this is very much reduced when focusing on the particle size. For the $(TiO_2)_n$ particles with O_h morphology a linear relationship exist between the particle height and $n^{1/3}$ (See Figure S3 in the supporting information). From this relationship one can readily find that the height of particles of 22810, 15000 and 10218 units is 18.1, 20.6 and 23.8 nm, respectively. Therefore one can safely conclude that the onset size for bulk-like electronic properties is of ~20 nm apical diameter in an anatase O_h nanoparticles exhibiting the most stable (101) surfaces; a prediction in full

agreement with previous indications extracted from significantly smaller nanoparticles.[47]

5. Conclusions

A systematic study has been presented of the atomic and electronic structure of realistic $(TiO_2)_n$ nanoparticles with $n \leq 455$ from relativistic, all electron density fucntional theory based calculations using a sufficiently large atom-centered numerical orbital basis set. Three different density functional have been used, each differing in the amount of Fock exchange included (0% in PBE to 25% in PBE0). Interestingly, the main conclusions regarding qualitative trends in relative stability and electronic structure are consistent and independent of the functional used.

The energy per TiO_2 unit ($\Delta E/n$) of the systems studied decreases as the size of the particle increases, as expected, with size effects dominating over morphology. In fact, octahedral and truncated octahedral nanoparticles exhibit similar size dependent stabilities. Note, however, that for very small sizes the truncated octahedral nanoparticles are similarly stable, or even more stable, than the octahedral nanoparticles. However, at larger sizes the effect of the different surfaces starts to become more important and the octahedral nanoparticles become more energetically stable than the truncated nanoparticles.

Comparing the level of theory used in the calculations and the different starting point geometries, we can see that nanoparticles directly cut from the bulk are highly metastable and still require significant optimization of their structure. Part of this structural relaxation is well captured by the tight-binding approach of Barnard et al.,[49] although further optimization at the PBE level still has a considerable effect on the structure and energetic stability.

Regarding the electronic structure, the main conclusions are that the optical gap only varies slightly with size whereas the electronic gap quickly converges with size to the value of the bulk band gap of anatase calculated at the same level of theory. This is confirmed by the explicit calculation of the exciton binding energy that shows smooth convergence towards zero (bulk behavior) for O_h particles of ~20 nm between the apical corner sites. This implies that nanoparticles of size equal or larger than the largest ones

studied in the present work would present electronic structure features, and hence photocatalytic activity, similar to that expected for bulk like anatase samples.

A final caveat is necessary here since the overall study presented in this work holds for TiO_2 nanoparticles in gas phase or in vacuum whereas photocatalysis, especially water splitting, takes place in aqueous environment. The presence of water will likely result in heavily hydroxylated nanoparticles with possible effects on both atomic and electronic structure trends. The effect of water on this type of nanoparticle is being currently studied in our laboratory.

Acknowledgements

The authors are very much indebted to Prof. Peter Zapol for having made available the TB-DFT optimized structures reported in ref. 49 and to Prof. Volker W. Blum for continuous support on efficient use of the FHI-AIMS code. This research was supported by the Spanish MINECO/FEDER CTQ2015-64618-R grant and, in part, by Generalitat de Catalunya (grants 2014SGR97 and XRQTC) and by the NOMAD Center of Excellence project, which received funding from the European Union's Horizon 2020 research and innovation programme under grant agreement No 676580. J.Y.L. acknowledges the financial support by Ministry of Science, ICT and Future Planning, subjected project to the project EDISON (Education-research Integration through Simulation On the Net, Grant No. 2012M3C1A6035359); K.C.K. acknowledges the financial support by Basic Science Research Program through the National Research Foundation of Korea (NRF) funded by the Ministry of Education (NRF-2016R1A6A3A11933303); O.L.G is grateful to the Universitat de Barcelona for a predoctoral grant; and, FI acknowledges additional support from the 2015 ICREA Academia Award for Excellence in University Research.Computational time at the Marenostrum supercomputer has been provided by the Barcelona Supercomputing Centre through grants from Red Española de Supercomputación and the COMPHOTOCAT project 2014112608 of the Partnership for Advanced Computing in Europe (PRACE).

Supporting information

The Supporting Information is available free of charge on the ACS Publications website at DOI: xxxxxxxxxxxxxx

Energy per unit for the bent and symmetric O_h nanoparticles

Formation energy of the O_h and TO_h particles as a function of size

Particle height as function of $n^{(1/3)}$ for the O_h particles

Cartesian coordinates of all TiO_2 particles as optimized at the PBE level using the NAO light-tier1 basis set

Table 1.- Total non relativistic PBE energy of the Ti atom (triplet state), O_2 (triplet state) and TiO_2 (singlet state) as obtained with a NAO light-tier1 and the GTO 6-311G** and TZVP basis sets.

	Total energy (Hartrees)		
	NAO (light-tier1)	6-311G**	TZVP
Ti	-848.3777	-848.3571	-848.3800
O_2	-149.6646	-149.6600	-149.6765
TiO_2	-998.1397	-998.0971	-998.1415
$Ti + O_2 \rightarrow TiO_2$	-0.0974	-0.0800	-0.0850

Figure 1. Schematic representation of the octahedral and cubo-octahedral TiO_2 anatase nanoparticles featuring (101) and (001) surfaces.

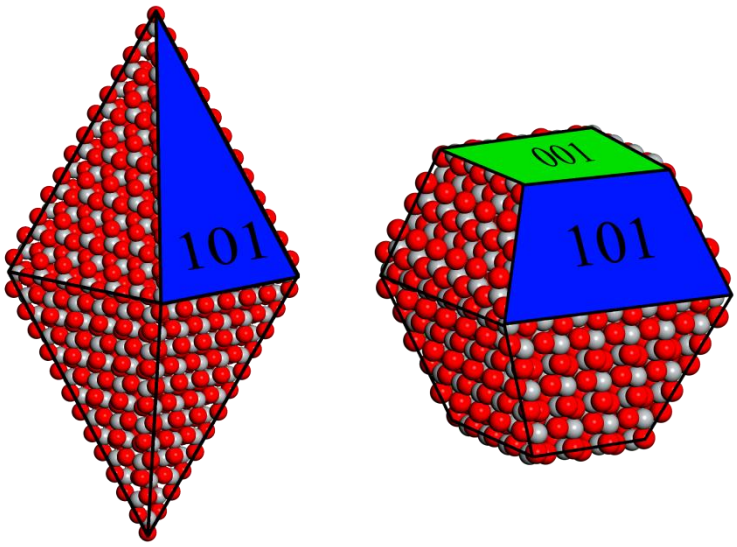

Figure 2. Octahedral (top) and cubo-octahedral (bottom) $(TiO_2)_n$ nanoparticles considered in the present work.

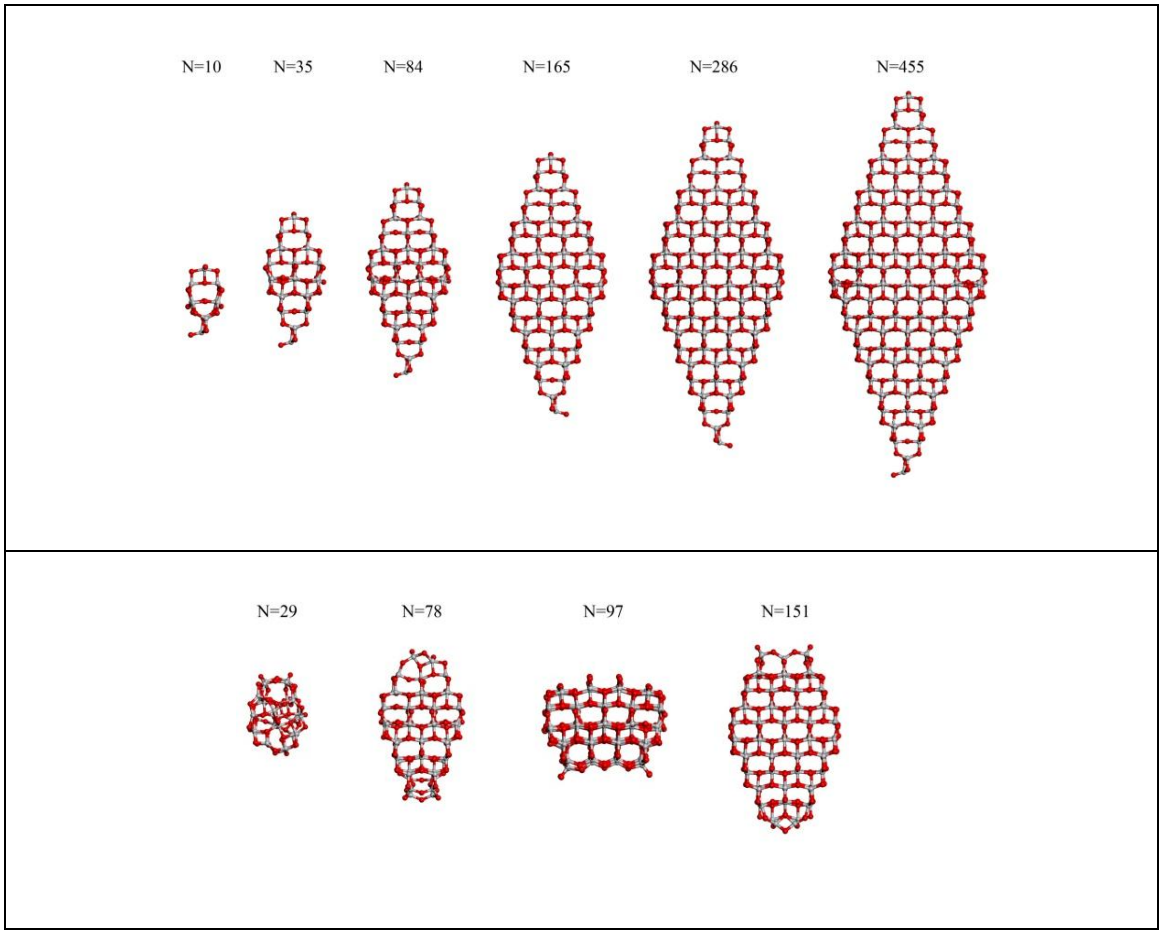

Figure 3. The two types of local minima found for the O_h type $(TiO_2)_n$ nanoparticles: tilted apical Ti-O bonds (left) and bulk-like straight apical Ti-O bonds (right)

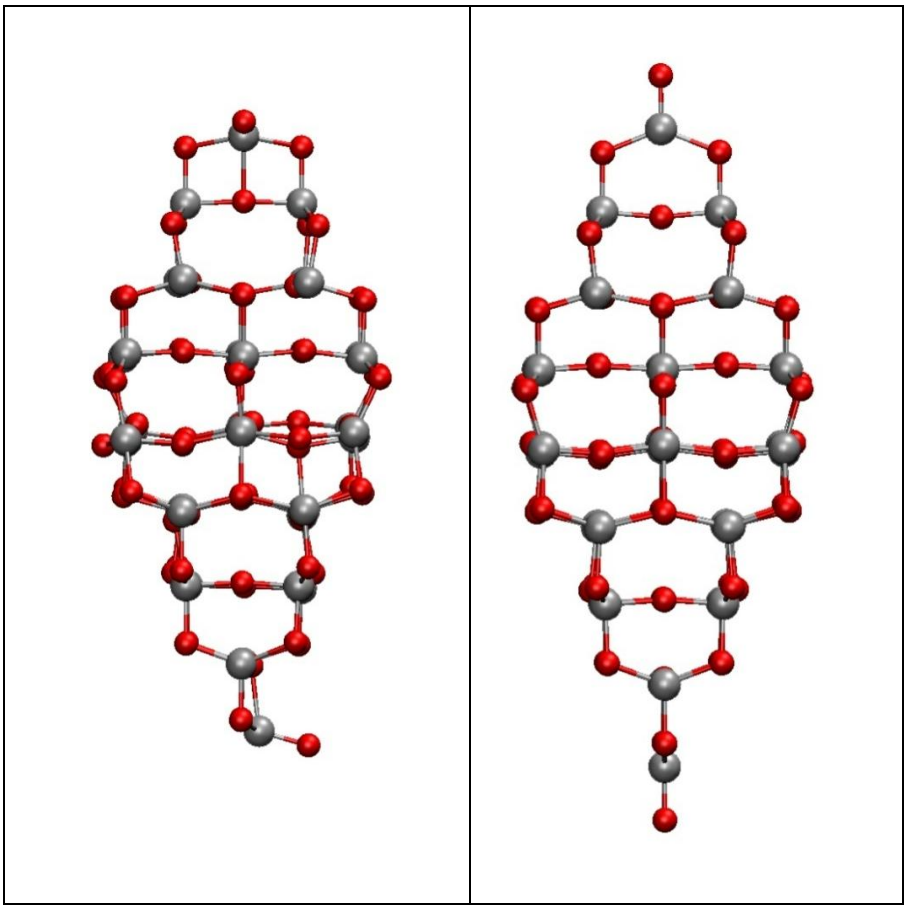

Figure 4. Energy per TiO_2 unit relative to anatase ($\Delta E/n$) for the different O_h and TO_h $(TiO_2)_n$ nanoparticles studied in the present work as obtained from calculations using the PBE functional. For comparison, the values corresponding to the unrelaxed structure cut from bulk and to the tight-binding relaxed structures from Barnard et al are also shown.[49] Blue squares correspond to single point calculations using the bulk cut structures (SP@BC), red dots correspond to single point calculations using the tight-binding relaxed structures (SP@TB), black diamonds correspond to the optimized O_h structures (Opt O_h), and green triangles correspond to the optimized TO_h structures (Opt TO_h).

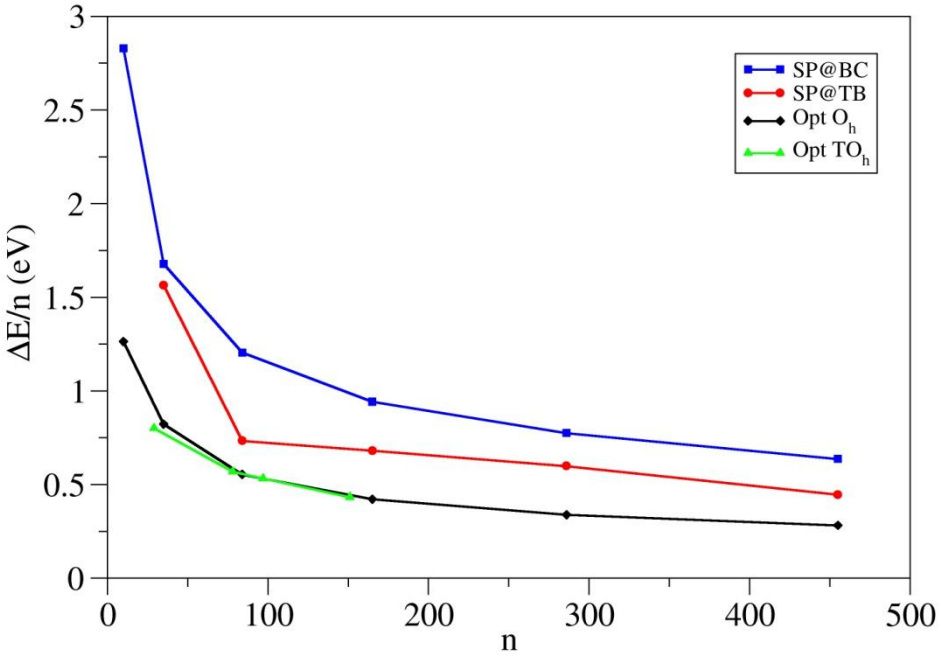

Figure 5. Average Ti-O distance (top panel), Ti coordination (middle panel) and O coordination (bottom panel) for the considered $(TiO_2)_n$ nanoparticles as a function of n. Black dots correspond to O_h and red squares to TO_h nanoparticles. The blue discontinuous lines correspond to the bulk values.

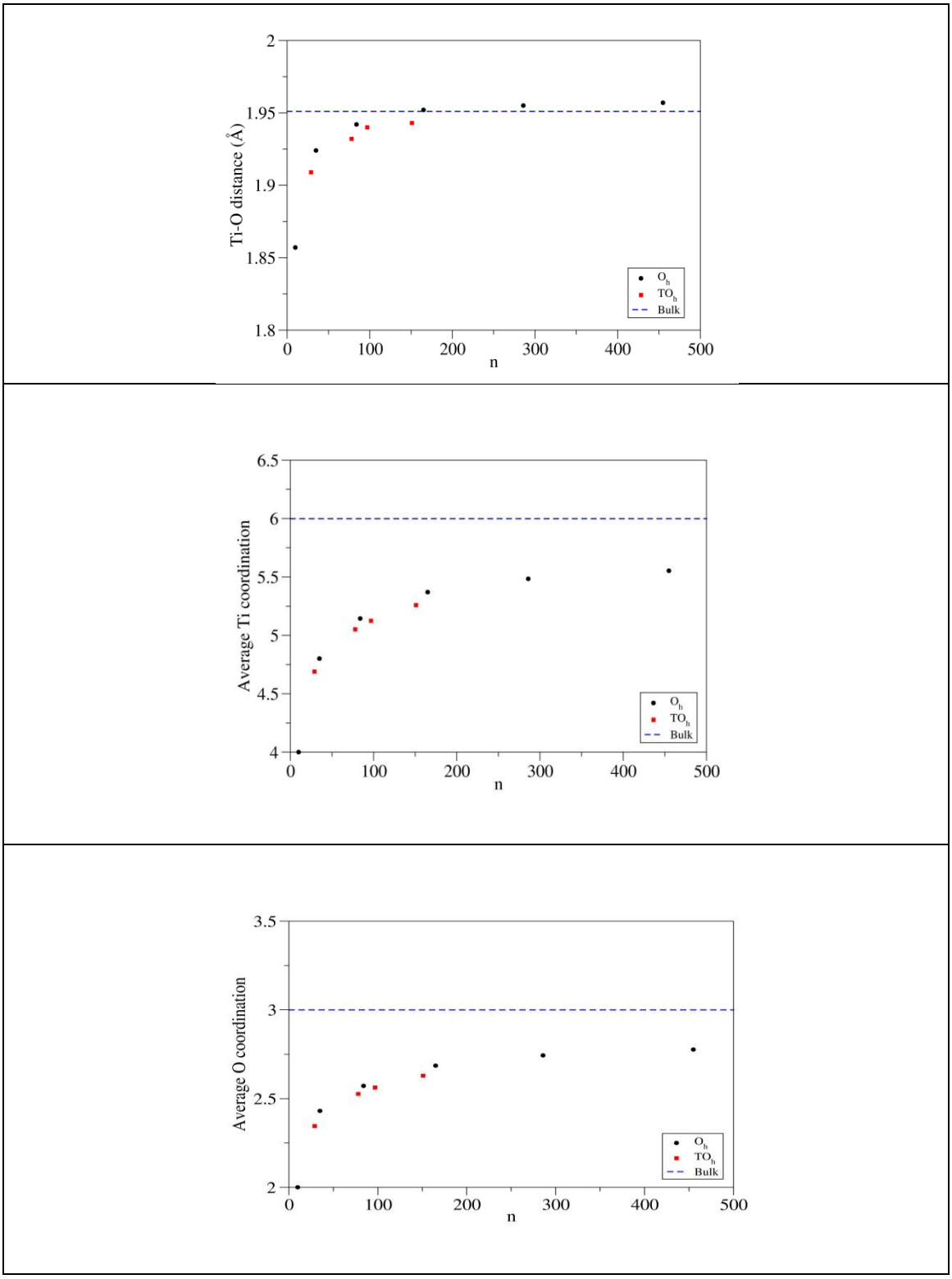

Figure 6. Optical (O_{gap}) and electronic (E_{gap}) gap calculated values for the octahedral $(TiO_2)_n$ nanoparticles as a function of n. Black, blue and red correspond to PBE, PBEx and PBE0 respectively at optimized PBE geometries. The discontinuous line refers to the bulk value calculated at the same level of theory

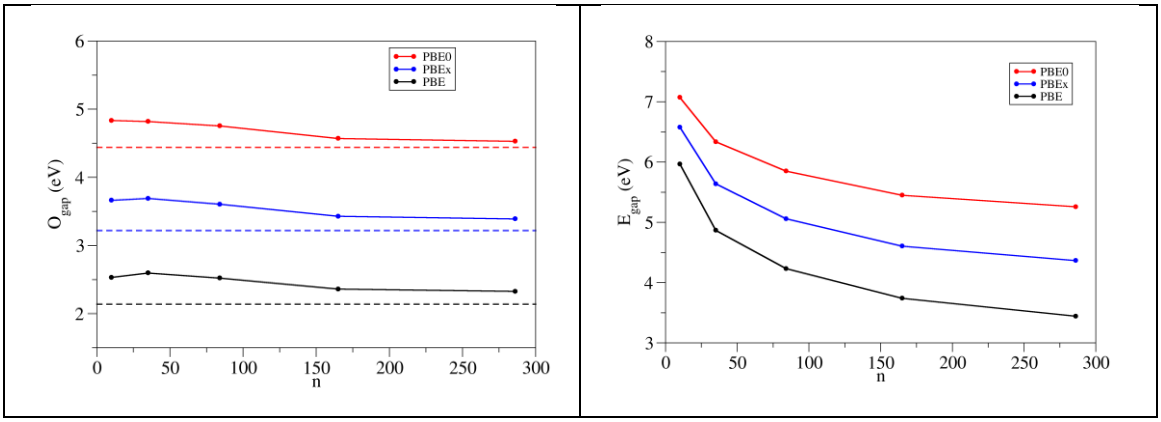

Figure 7. Optical (O_{gap}) and electronic (E_{gap}) gap calculated values for the whole set of $(TiO_2)_n$ nanoparticles, O_h and TO_h, as a function of n as predicted from the PBEx calculations at the PBE optimized geometry. Black dots and red squares refer to O_{gap} for O_h and TO_h nanoparticles, respectively. Green diamonds and blue triangles correspond to E_{gap} values for O_h and TO_h nanoparticles, respectively.

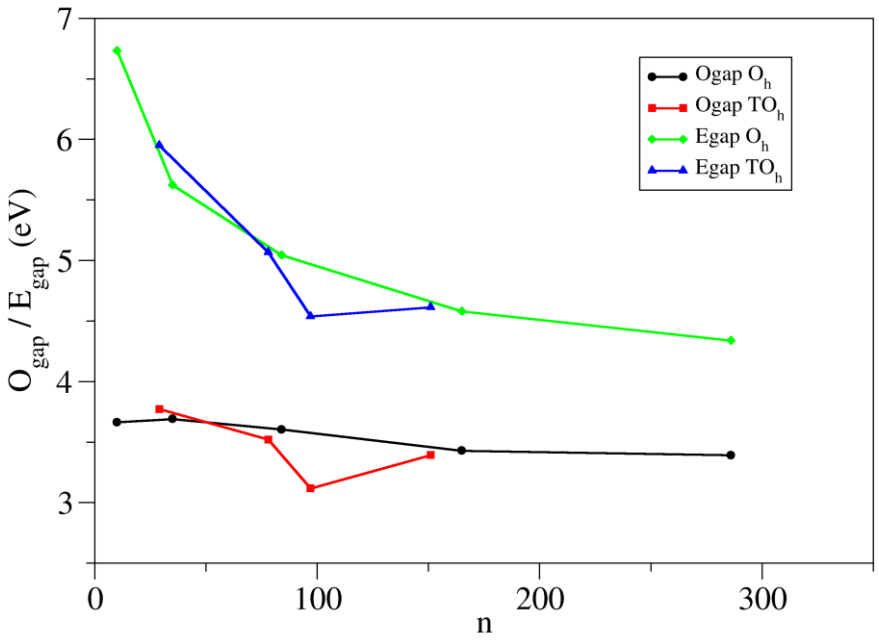

Figure 8. Exciton binding energy for the whole set of $(TiO_2)_n$ nanoparticles, O_h and TO_h, as a function of n as predicted from the different considered density functionals. Black dots, red squares and blue diamonds correspond to O_h nanoparticles at PBE, PBEx and PBE0 levels, respectively. Green triangles correspond to PBEx results for TO_h nanoparticles.

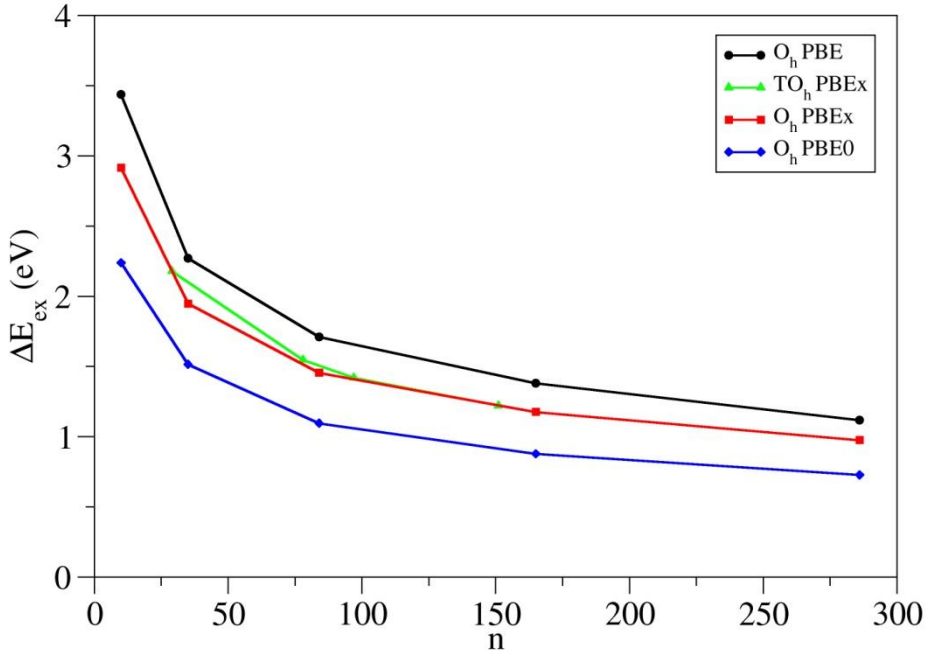

Figure 9. Exciton binding energy for the O_h set of $(TiO_2)_n$ nanoparticles as a function of $n^{-1/3}$ as predicted from the PBE0 and PBEx hybrid density functionals. Red circles and green triangles correspond values obtained with the PBE0 and PBEx hybrid functionals, respectively. Blue lines correspond to the non-relativistic B3LYP/6-31G(d) values for a set of smaller particles (upper blue line) and to the values scaled by 20% (bottom blue line) to take into account the overestimation of the band gap at the B3LYP level as taken from Ref. 47.

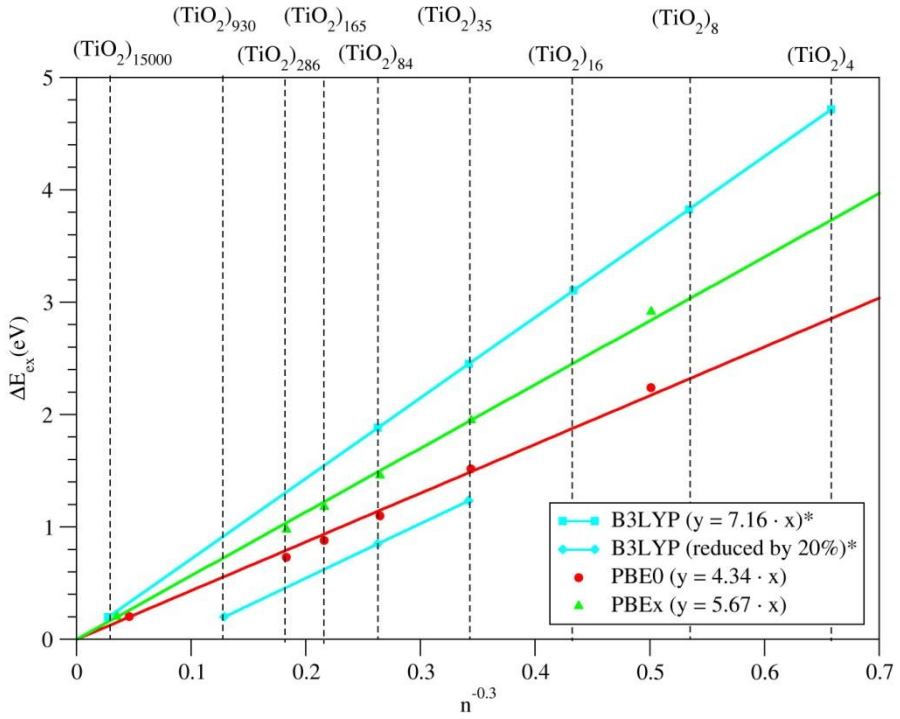

References:

(1) Chen, X.; Mao, S. S. Titanium Dioxide Nanomaterials: Synthesis, Properties Modifications and Applications. *Chem. Rev.* **2007**, *107*, 2891–2959.

(2) Oregan, B.; Gratzel, M. A Low-Cost, High-Efficiency Solar Cell Based on Dye-Sensitized Colloidal TiO_2 Films *Nature*, **1991**, *353*, 6346, 737-740.

(3) Gratzel, M. Photoelectrochemical Cells, *Nature*, **2001**, *414*, 6861 338-344.

(4) Hoffmann, M. R.; Martin, S. T.; Choi, W.; Bahnemann, D. W. Environmental Applications of Semiconductor Photocatalysis. *Chem. Rev.* **1995**, *95*, 69–96.

(5) Mill, A.; Davies, R. H.; Worsley, D. Water-Purification by Semiconductor Photocatalysis. *Chem. Soc. Rev.* **1993**, *22*, 417–425.

(6) Yaghoubi, H.; Taghavinia, N.; Alamdari Eskandar K. Self Cleaning TiO_2 Coating on Polycarbonate: Surface Treatment, Photocatalytic and Nanomechanical Properties. Surf. Coat. Technol. **2010**, *204*, 1562-1568.

(7) Fox, M. A.; Dulay, M. T. Heterogeneous Photocatalysis. *Chem. Rev.* **1993**, *93*, 341–357.

(8) Xu, H.; Ouyang, S.; Liu, L.; Reunchan, P.; Umezawa, N.; Ye, J. Recent Advances in TiO_2-Based Photocatalysis. *J. Mater. Chem. A* **2014**, *2*, 12642−12661.

(9) Hashimoto, K.; Irie, H.; Fujishima, A. TiO_2 Photocatalysis: A Historical Overview and Future Prospects. *Jpn. J. Appl. Phys*. **2005**, *44*, 8269–8285.

(10) Fujishima, A.; Zhang, X.; Tryk, D. A. TiO_2 Photocatalysis and Related Surface Phenomena. *Surf. Sci. Rep.* **2008**, *63*, 515–582.

(11) Chen, X. B.; Shen, S. H.; Guo, L. J.; Mao, S. S. Semiconductor-Based Photocatalytic Hydrogen Generation. *Chem. Rev.* **2010**, *110*, 6503–6570.

(12) Kudo, A.; Miseki, Y. Heterogeneous Photocatalyst Materials for Water Splitting. *Chem. Soc. Rev.* **2009**, *38*, 253–278.

(13) Kavan, L.; Gratzel, M.; Gilbert, S. E.; Klemenz, C.; Scheel, H. J. Electrochemical and Photoelectrochemical Investigation of Single-Crystal Anatase. *J. Am. Chem. Soc.* **1996**, *118*, 6716-6723.

(14) Fernandez-Garcia, M.; Martinez-Arias, A.; Hanson, J. C.; Rodriguez, J. A. Nanostructured Oxides in Chemistry: Characterization and Properties. *Chem. Rev.* **2004**, *104*, 4063.

(15) Asahi, R.; Morikawa, T.; Ohwaki, T.; Aoki, K.; Taga, Y. Visible-Light Photocatalysis in Nitrogen-doped Titanium Oxides. *Science* **2001**, *293*, 269-271.

(16) Asahi, R.; Morikawa, T.; Irie, H.; Ohwaki, T. Nitrogen-Doped Titanium Dioxide as Visible-Light-Sensitive Photocatalyst: Designs, Developments, and Prospects. *Chem. Rev.* **2014**, *114*, 9824-9852.

(17) Calatayud, D.; Jardiel, T.; Peiteado, M.; Illas, F.; Giamello, E.; Palomares, F.; Fernández Hevia, D.; Caballero, A. Synthesis and Characterization of Blue Faceted Anatase Nanoparticles Through Extensive Fluorine Lattice Doping. *J. Phys. Chem. C* **2015**, *119*, 21243-21250.

(18) Pelaez, M.; Nolan, N. T.; Pillai S. C.; Seery M. K.; Falaras P.; Kontos A. G.; Dunlop P. S. M.; Hamilton J. W. J.; Byrne J.A.; O'Shea, K.; Entezarig M. H., Dionysioua D. D. A Review on the Visible Light Active Titanium Dioxide Photocatalysts for Environmental Applications. *Appl. Catal. B.* **2012**, *125*, 331-349.

(19) Hoffmann, M. R.; Martin, S. T.; Choi, W.; Bahnemann, D. W. Environmental Applications of Semiconductor Photocatalysis. *Chem. Rev.* **1995**, *95*, 69-96.

(20) Fox, M. A.; Dulay, M. T. Heterogeneous Photocatalysis. *Chem. Rev.* **1993**, *93*, 341-357.

(21) Ravelli, D.; Dondi, D.; Fagnoni, M.; Albini, A. Photocatalysis. A Multi-faceted Concept for Green Chemistry. *Chem. Soc. Rev.* **2009**, *38*, 1999−2011.

(22) Yuliati, L.; Yoshida, H. Photocatalytic Conversion of Methane. *Chem. Soc. Rev.* **2008**, *37*, 1592-1602.

(23) Liu, G.; Yang, H. G.; Pan, J.; Yang, Y. Q.; Lu, G. Q. (Max); Cheng, H. M. Titanium Dioxide Crystals with Tailored Facets. *Chem. Rev.* **2014**, *114*, 9559-9612.

(24) Mattioli, G.; Filippone, F.; Alippi, P.; Bonapasta, A. Ab Initio Study of the Electronic States Induced by Oxygen Vacancies in Rutile and Anatase TiO_2. *Phys. Rev. B* **2008**, *78*, 241201.

(25) Di Valentin, C.; Pacchioni, G. Spectroscopic Properties of Doped and Defective Semiconducting Oxides from Hybrid Density Functional Calculations. *Acc. Chem. Res.* **2014**, *47*, 3233-3241.

(26) Morgan, B. J.; Watson, G. W. Intrinsic n-type Defect Formation in TiO_2: A Comparison of Rutile and Anatase from GGA+U Calculations. *J. Phys. Chem. C* **2010**, *114*, 2321-2328.

(27) Stausholm-Møller, J.; Kristoffersen, H. H.; Hinnemann, B.; Madsen, G. K. H.; Hammer, B. DFT+U Study of Defects in Bulk Rutile TiO_2. *J. Chem. Phys.* **2010**, *133*, 144708.

(28) Mattioli, G.; Alippi, P.; Filippone, F.; Caminiti, R.; Bonapasta, A. Deep versus Shallow Behavior of Intrinsic Defects in Rutile and Anatase TiO_2 Polymorphs. *J. Phys. Chem. C* **2010**, *114*, 21694-21704.

(29) Finazzi, E.; Di Valentin, C.; Pacchioni, G.; Selloni, A. Excess Electron States in Reduced Bulk Anatase TiO_2: Comparison of Standard GGA, GGA+U, and Hybrid DFT Calculations. *J. Chem. Phys.* **2008**, *129*, 154113.

(30) Islam, M. M.; Bredow, T.; Gerson, A. Electronic Properties of Oxygen-Deficient And Aluminum-Doped Rutile TiO_2 from First Principles. *Phys. Rev. B* **2007**, *76*, 045217.

(31) Janotti, A.; Varley, J. B.; Rinke, P.; Umezawa, N.; Kresse, G.; Van de Walle, C. G. Hybrid Functional Studies of the Oxygen Vacancy in TiO_2. *Phys. Rev. B* **2010**, *81*, 085212.

(32) Deák, P.; Aradi, B.; Frauenheim, T. Quantitative Theory of the Oxygen Vacancy and Carrier Self-Trapping in Bulk TiO_2. *Phys. Rev. B* **2012**, *86*, 195206.

(33) Tosoni, S.; Lamiel-Garcia, O.; Fernández-Hevia, D.; Doña, J. M.; Illas, F. Electronic Structure of F-doped Bulk Rutile, Anatase and Brookite Polymorphs of TiO_2, *J. Phys. Chem. C*, **2012**, *116*, 12738-12746.

(34) Lazzeri, M.; Vittadini, A.; Selloni, A. Structure and Energetics of Stoichiometric TiO_2 Anatase Surfaces. *Phys. Rev. B* **2001**, *63*, 155409.

(35) Gong, X. Q.; Selloni, A. Reactivity of Anatase TiO_2 Nanoparticles: The Role of the Minority (001) surface. *J. Phys. Chem. B* **2005**, *109*, 19560-19562.

(36) Morgan, B. J.; Watson, G. W. A DFT+U Description of Oxygen Vacancies at the TiO_2 Rutile (110) Surface. *Surf. Sci.* **2007**, *601*, 5034-5041.

(37) Auvinen, S.; Alatalo, M.; Haario, H.; Jalava, J. P.; Lamminmäki, R. J. Size and Shape Dependence of the Electronic and Spectral Properties in TiO_2 Nanoparticles. *J. Phys. Chem. C* **2011**, *115*, 8484-8493.

(38) Li, S. G.; Dixon, D. A. Molecular Structures and Energetics of the (TiO2)n (n=1-4) clusters and their anions. *J. Phys. Chem. A* **2008**, *112*, 6646-6666.

(39) Aguilera-Granja, F.; Vega, A.; Balbas, L. C. New structural and electronic properties of $(TiO_2)_{10}$. *J. Chem. Phys.* **2016**, *144*, 234312.

(40) Auvinen, S.; Alatalo, M.; Haario, H.; Vartiainen, E.; Jalava, J. P.; Lamminmaki, R. J. Refractive Index Functions of TiO_2 Nanoparticles. *J. Phys. Chem. C* **2013,** *117*, 3503-3512,

(41) Berardo, E.; Hu, H. S.; van Dam, H. J. J.; Shevlin, S. A.; Woodley, S. M.; Kowalski, K.; Zwijnenburg, M. A. Describing Excited State Relaxation and Localization in TiO2 Nanoparticles Using TD-DFT. *J. Chem. Theory Comput.* **2014,** *10*, 5538-5548.

(42) Persson, P.; Christof, J.; Gebhardt, M.; Lunell, S. The Smallest Possible Nanocrystals of Semiionic Oxides. *J. Phys. Chem. B*, **2003**, *107*, 3336-3339.

(43) Shevlin, S. A.; Woodley, S. M. Electronic and Optical Properties of Doped and Undoped $(TiO_2)_n$ Nanoparticles. *J. Phys. Chem. C* **2010**, *114*, 17333-17343

(44) Fernando, A.; Dimuthu, K. L.; Weerawardene, M.; Karimova, N. V.; C. M. Quantum Mechanical Studies of Large Metal, Metal Oxide, and Metal Chalcogenide Nanoparticles and Clusters. *Chem. Rev.* **2015**, *115*, 6112-6216.

(45) Berardo, E.; Hu, H. S.; Shevlin, S. A.; Woodley, S. M.; Kowalski, K.; Zwijnenburg, M. A. Modeling Excited States in TiO_2 Nanoparticles: On the

Accuracy of a TD-DFT Based Description. *J. Chem. Theory Comput.* **2014**, *10*, 1189-1199.

(46) Buckeridge, J.; Butler, K. T.; Catlow, C. R. A.; Logsdail, A. J.; Scanlon, D. O.; Shevlin, S. A.; Woodley, S. M.; Sokol, A. A.; Walsh, A. Polymorph Engineering of TiO_2: Demonstrating How Absolute Reference Potentials Are Determined by Local Coordination. *Chem. Mater.* **2015**, *27*, 3844–3851.

(47) Cho, D.; Ko, K. C.; Lamiel García, O.; Bromley, S. T.; Lee, J. Y.; Illas, F. Effect of Size and Structure on the Ground and Excited State Electronic Structure of TiO_2 Nanoparticles. *J. Chem. Theory Comput.* **2016**, *12*, 3751-3763.

(48) O. Lamiel Garcia, A. Cuko, M. Calatayud, F. Illas, S. T. Bromley. Predicting Size-Dependent Emergence of Crystallinity in Nanomaterials: Titania Nanoclusters Versus Nanocrystals. *Nanoscale*, **2017**, *9*, 1049-1058

(49) Barnard, A. S.; Erdin, S.; Lin, Y.; Zapol, P.; Halley, J. W. Modeling the Structure and Electronic Properties of TiO_2 Nanoparticles. *Phys. Rev. B* **2006**, *73*, 205405.

(50) Blum, V.; Gehrke, R.; Hanke, F.; Havu, P.; Havu, V.; Ren, X.; Reuter, K.; Scheffler, M. Ab Initio Molecular Simulations with Numeric Atom-centered Orbitals. *Comput. Phys. Commun.* **2009**, *180*, 2175–2196.

(51) Havu V.; Blum V.; Havu P.; and Matthias S. Efficient O(N) Integration for All-electron Electronic Structure using Numerically Tabulated Basis Functions. *J. Comput. Phys.* **2009**, *228*, 8367-8379.

(52) Ren X.; Rinke P.; Blum V.; Wieferink J.; Tkatchenko A.;, Sanfilippo A.; Reuter K.; Scheffler M.; Resolution-of-identity Approach to Hartree-Fock, Hybrid Density Functionals, RPA, MP2, and GW with Numeric Atom-centered Orbital Basis Functions. *New J. Phys*. **2012**, *14*, 053020.

(53) Chang C., Pelissier M.; Durand M. Regular Two-Component Pauli-Like Effective Hamiltonians in Dirac Theory. *Phys. Scr.* **1986**, *34*, 394.

(54) van Lenthe E.; Baerends E. J.; Snijders J. G. Relativistic Regular Two-component Hamiltonians *J. Chem. Phys.* **1993**, *99*, 4597.

(55) Perdew J.P.; Burke K.; Ernzerhof M. Generalized Gradient Approximation Made Simple. *Phys. Rev. Lett.* **1996**, *77*, 3865-3868.

(56) The tight-binding structures were kindly provided by Peter Zapol, private communication.

(57) Sousa, C.; Tosoni, S.; Illas, F. Theoretical Approaches to Excited States Related Phenomena in Oxide Surfaces. *Chem. Rev.* **201**3, *113*, 4456-4495.

(58) Ko K. C.; Lamiel-García O.; Lee J. Y. Illas F. Performance of a Modified Hybrid Functional in the Simultaneous Description of Stoichiometric and Reduced TiO_2 Oolymorphs *Phys. Chem. Chem. Phys.*, **2016**, *18*, 12357

(59) Kim, S.; Ko, K. C.; Lee, J. Y.; Illas, F., Single oxygen vacancies of $(TiO_2)_{35}$ as a prototype reduced nanoparticle: implication for photocatalytic activity. *Phys. Chem. Chem. Phys*. **2016**, *18*, 23755.

(60) Wulff, G. On the question of speed of growth and dissolution of crystal surfaces. *Z. Krist.* **1901**, 34, 449-530.

(61) Bromley, S. T.; Moreira, I. De P.R.; Neyman, K-M.; Illas, F. Approaching nanoscale oxides: models and theoretical methods. *Chem. Soc. Rev.* **2009**, *38*, 2657-2670.

(62) Lazzeri, M.; Vittadini, A.; Selloni, A., Structure and energetics of stoichiometric TiO_2 anatase surfaces. *Phys. Rev. B* **2001**, *63*, 155409.

(63) Yang, H. G.; Sun, C. H.; Qiao, S. Z.; Zou, J.; Liu, G.; Smith, S. C.; Cheng, H. M.; Lu, G. Q. Anatase TiO_2 Single Crystals with a Large Percentage of Reactive Facets. *Nature* **2008**, *453*, 638-641

(64) Lamiel-Garcia O.; Tosoni, S.; Illas, F. Relative Stability of F-Covered TiO_2 Anatase (101) and (001) Surfaces from Periodic DFT Calculations and ab Initio Atomistic Thermodynamics. *J. Phys. Chem. C*, **2014**, *118*, 13667-13673.

(65) Bondi, A. van der Waals Volumes and Radii. *J. Phys. Chem.* **1964**, *68*, 441.

(66) Duanmu, K.; Friedrich, J.; Truhlar, D. G. Thermodynamics of Metal Nanoparticles: Energies and Enthalpies of Formation of Magnesium Clusters and Nanoparticles as Large as 1.3 nm. *J. Phys. Chem. C* **2016**, *120*, 26110–26118.

(67) Di Valentin, C.; Finazzi, E.; Pacchioni, G.; Selloni, A.; Livraghi, S.; Paganini, M.C.; Giamello, E. N-doped TiO_2: Theory and experiment. *Chem. Phys*, **2007**, *339*, 44-56.

(68) Zhang, Z.; Yates, J. T. Jr.; Band bending in semiconductors: chemical and physical consequences at surfaces and interfaces. *Chem. Rev.* **2012**, *112*, 5520-5551.

(69) Pascual, J.; Camassel, J.; Mathieu, H. Fine Structure in the Intrinsic Absorption Edge of TiO_2. *Phys. Rev. B* **1978**, *18*, 5606–5614.

(70) Tang, H.; Levy, F.; Berger, H.; Schmid, P. E. Urbach tail of anatase TiO_2, *Phys. Rev. B* **1995**, *52*, 7771-7774.

(71) Kang, W.; Hybertsen, M. S. Quasiparticle and Optical Properties of Rutile and Anatase TiO_2. *Phys. Rev. B* **2010**, *82*, 085203.

(72) Almquist, C. B.; Biswas, P., Role of Synthesis Method and Particle Size of Nanostructured TiO_2 on Its Photoactivity. *J. Catal.* **2002**, *212*, 145-156.

Graphic for TOC